Transfer lengths and spin injection from a three-dimensional ferromagnet into graphene

Z. G. Yu,* J. Baker, and S. Krishnamurthy
Physical Sciences Division, SRI International, 333 Ravenswood Avenue, Menlo Park, California 94025, USA
(Received 26 February 2010; revised manuscript received 23 April 2010; published 16 July 2010)

In graphene spintronic devices, spin currents are injected and probed by three-dimensional ferromagnetic electrodes on a two-dimensional graphene layer. Here we develop a unified theory to understand the observed spin-injection signals and their dependence on a dc-bias current in these devices by different groups. The spin-dependent transfer length, which measures the length required for a current to change from lateral in graphene to vertical in the electrode, is found to play a central role in determining the spin-current distribution as well as the signal fidelity. The theory consistently explains the experiments and suggests that the observed dc-bias dependence is due not to change in the spin-injection efficiency but to redistribution of the spin current near the ferromagnetic electrode.

DOI: 10.1103/PhysRevB.82.035425 PACS number(s): 72.25.Hg, 73.63.−b

I. INTRODUCTION

Recent demonstration of large spin injection from a ferromagnetic electrode into graphene,[1,2] together with graphene's outstanding transport attributes,[3,4] suggest a promising potential of graphene-based spintronic devices. Spin injection from ferromagnets into nonmetallic systems has attracted considerable attention because of its importance in spintronic devices as well as its fascinating physics.[5,6] The extensive research on this topic resulted in several insightful concepts. For example, the conductivity mismatch between a ferromagnet and a semiconductor[7] is found to prevent an efficient spin injection, which, however, can be overcome by using spin-selective interfacial resistance.[8–10] In addition, an electrical field can significantly modify spin diffusion and result in nonlinear spin-transport behaviors in semiconductors.[11]

Spin injection into graphene was mostly studied in a nonlocal structure, where the spin-injection signal (voltage) is probed in a separate circuit than the current injection circuit.[12] By using the ac lock-in technique, the nonlocal spin-injection signal is found to depend strongly on an applied dc bias (nonlinear spin transport) in devices with an Al_2O_3 layer between Co and graphene[13] and devices with a transparent interface.[14] In the latter, the dc-bias dependence is much stronger for *p*-type graphene than for *n* type. However, no such an asymmetry between electron and hole is observed in the former. Possible pin holes in the Al_2O_3 layer were invoked to explain the bias effect.[13] The observed electron-hole asymmetry for a transparent interface remains unexplained. Nonlinear spin transport is important in that it allows a thorough comparison between theory and experiment. To date, no systematic theory is available to describe spin injection and nonlinear spin transport in graphene devices. Here we develop such a theory and show that the observed spin transport in both kinds of devices can be consistently modeled, without resorting to pin holes (which do not exist in a transparent interface), by properly describing contact between three-dimensional (3D) electrode and two-dimensional (2D) graphene, and, in particular, its spin-dependent transfer lengths, which are short in the transparent-interface devices but long in the devices with Al_2O_3. We find that these transfer lengths largely determine efficacy of spin injection and detection. Numerical simulations also indicate that the geometry of a 3D ferromagnet in all-metal nonlocal structures can affect the spin signals,[15,16] suggesting that the concept of spin-dependent transfer lengths introduced in this paper can be extended to other lateral spintronic devices. Hence it is important to experimentally characterize these transfer lengths in ferromagnet/graphene contacts and other lateral spin-injection structures, through, for example, the dependence of contact resistance on the contact size.

The paper is organized as follows. First, we introduce in Sec. II the concept of spin-dependent transfer length at a ferromagnet/graphene contact and derive relations between spin-polarized electrochemical potential and current at the edges of the contact. Then we examine how the spin-dependent transfer length affect spin injection in Sec. III and spin detection in Sec. IV, respectively. In Sec. V, we study nonlinear spin-injection signals in nonlocal structures under different bias currents and compare calculations with experiment. Finally, we summarize our results in Sec. VI.

II. SPIN-DEPENDENT TRANSFER LENGTH

The concept of transfer length was originally introduced in semiconductor field-effect transistors, where source and drain contacts are on top of a thin semiconductor channel.[17] Here we extend this concept to magnetic contacts. Consider a ferromagnetic electrode on top of a graphene sheet with a current injected from the electrode into graphene (along the z axis). The injected current flows in graphene along the x axis and the width of the graphene sheet, w, is perpendicular to the x axis. The spin-polarized current, I_s, in graphene at x is

$$I_s(x) = w\frac{1}{R^s_\square}\frac{d\mu_s(x)}{dx}. \quad (1)$$

Here μ_s is the spin-polarized electrochemical potential and $s=\uparrow$ or $\downarrow$ represents spin polarization. $R^s_\square$ is the graphene sheet resistance for spin s. When the magnetic proximity is neglected, $R^s_\square=2R_\square$ with $R_\square$ being the sheet resistance of graphene. Because of the current injection, from x to $x+dx$, the current will increase by an amount of

$$dI_s = wdx[\mu_s(x) - \mu_s^f]/\rho_c^s \equiv wdx\Delta\mu_s(x)/\rho_c^s, \quad (2)$$

where ρ_c^s is the spin-dependent intrinsic contact resistivity, which arises from carrier thermionic emission and/or tunneling and is present even without an interfacial layer between electrodes and graphene and μ_s^f is the spin-dependent electrochemical potential at the electrode surface next to the graphene ($z=0$). The value μ_s^f is independent of x because in the electrode the current is presumably along the z direction. From Eqs. (1) and (2) and neglecting spin flipping within the graphene region underneath the electrode, we obtain

$$\frac{d^2\Delta\mu_s(x)}{dx^2} - \frac{\Delta\mu_s(x)}{L_s^2} = 0, \quad (3)$$

where $L_s=(\rho_c^s/R_\square^s)^{1/2}$ is the transfer length for spin s, which measures how fast the current transfers from under the contact (lateral) into the contact (vertical). For a magnetic electrode, $L_\uparrow \neq L_\downarrow$, indicating that up-spin and down-spin currents have different paths when injected from the electrode to graphene.

For a finite electrode located at $-a_0<x<0$, the general solution to Eq. (3) is $\Delta\mu_s(x)=Ae^{-x/L_s}+Be^{(x+a_0)/L_s}$, and from Eq. (1), it can readily be verified that

$$I_s(x) = I_s(0)\cosh\frac{x}{L_s} + \Delta\mu_s(0)\frac{w}{R_\square^s L_s}\sinh\frac{x}{L_s}, \quad (4)$$

$$\Delta\mu_s(x) = \Delta\mu_s(0)\cosh\frac{x}{L_s} + I_s(0)\frac{R_\square^s L_s}{w}\sinh\frac{x}{L_s}. \quad (5)$$

These are nothing but the transmission line equations of the circuit shown in Fig. 1, where $G=(w/\rho_c^s)$ and $R=R_\square^s/w$. We emphasize that there is a significant distinction between the contact resistance for charge and spin transport. For charge transport the current outside the circuit must be zero. Whereas for spin transport, up-spin and down-spin currents are finite and opposite in sign outside the current circuit, which is, in fact, the foundation of nonlocal spin detection. The contact resistance obtained from resistance measurements is

$$\frac{1}{R_c} = \sum_s \left.\frac{I_s(0)}{\Delta\mu_s(0)}\right|_{I_s(-a_0)=0} = \sum_s \frac{w}{2R_\square L_s}\tanh\frac{a_0}{L_s}, \quad (6)$$

which is not scaled with the contact size a_0. Equation (6) suggests that the spin-dependent transfer lengths can be determined by measuring R_c as a function of a_0.

III. TRANSFER LENGTH AND SPIN INJECTION

Now we examine how the spin-dependent transfer lengths affect spin injection. We consider a current of I_0+I injected into graphene from an electrode at $-a_0<x<0$ (the other electrode in the current circuit is assumed at $x=\infty$), where I_0 is a dc-bias current and I is a low-frequency ac, and study the spin-injection signals at the same ac frequency. The dc-bias current gives rise to an electric field $E=d\mu_0/dx=I_0R_\square/w$, where μ_0 is the average (spin-independent) electrochemical potential in graphene. Spin transport in graphene was experimentally found[18] to quantitatively follow the spin drift-diffusion equation derived for semiconductors, which can be written in terms of spin-dependent electrochemical potentials[11]

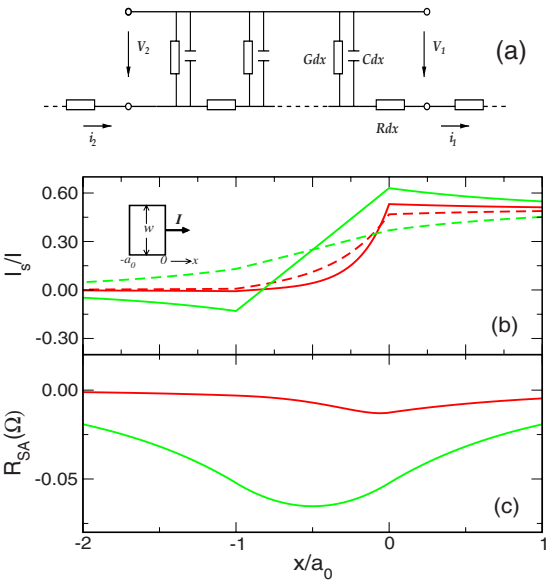

FIG. 1. (Color online) (b) Spin-dependent currents and (c) spin accumulation as a function of location in a ferromagnet/graphene structure. The inset of panel (b) shows a top view of the ferromagnet from which an electrical current is injected into graphene and flows to right ($x>0$). Panel (a) shows an equivalent circuit for an electrode/graphene contact. Solid (dashed) lines in panel (b) describe the up-spin (down-spin) current. Red (dark gray) and green (light gray) curves correspond to $L_\uparrow=0.2a_0$ and $5a_0$, respectively. $L_\downarrow/L_\uparrow=1.8$, $a_0=1$ μm, $\sigma^f=1.7\times10^5$, $L_f=50$ nm, $L=1$ μm, $(\sigma_\uparrow^f-\sigma_\downarrow^f)/\sigma^f=0.5$, and $R_\square=1$ kΩ.

$$\frac{d^2(\mu_\uparrow-\mu_\downarrow)}{dx^2} + \frac{\nu E}{D}\frac{d(\mu_\uparrow-\mu_\downarrow)}{dx} - \frac{\mu_\uparrow-\mu_\downarrow}{L^2} = 0, \quad (7)$$

where ν is the carrier mobility, D is the diffusion constant, E is the applied electric field, and L is the intrinsic spin-diffusion length. For ferromagnetic electrodes, the second term in the above equation can be neglected and Eq. (7) becomes the conventional spin-diffusion equation.[19] The ac signals in graphene are $\mu_{\uparrow(\downarrow)}=+(-)ae^{-x/L_e}+\frac{I}{w}R_\square x$ for $x>0$, where $L_e=[+(-)\nu E/2D+\sqrt{(\nu E/2D)^2+(1/L)^2}]^{-1}$ for holes (electrons), is the upstream (when $L_e>L$) or downstream (when $L_e<L$) spin-diffusion length,[11] and $\mu_{\uparrow(\downarrow)}=+(-)be^{(x+a_0)/L}+w_1$ for $x<-a_0$. The electrochemical potentials in the electrode are $\mu_{\uparrow(\downarrow)}(z)=\mu_0^f+\frac{zI}{\sigma^f w a_0}+(-)c^f\frac{\sigma^f}{\sigma_{\uparrow(\downarrow)}^f}e^{-z/L_f}$, where L_f is the spin-diffusion length in the electrode, $\sigma_{\uparrow(\downarrow)}^f$ is the up-spin (down-spin) conductivity of the electrode, and $\sigma^f=\sigma_\uparrow^f+\sigma_\downarrow^f$. The five unknowns, μ_0^f, c^f, w_1, a, and b, can be completely determined from the four relations between $\Delta\mu_s$ and I_s at the two contact edges $x=0$ and $x=-a_0$ according to Eqs. (4) and (5), and the spin-current conservation, $(I_\uparrow-I_\downarrow)_{z=0}=(I_\uparrow-I_\downarrow)_{x=-a_0}-(I_\uparrow-I_\downarrow)_{x=0}$.

The spin current in the magnetic electrode at $z=0$ is $I_{\uparrow(\downarrow)}|_{z=0}=a_0\sigma_{\uparrow(\downarrow)}^f\frac{d\mu_{\uparrow(\downarrow)}^f(0)}{dz}=\frac{\sigma_{\uparrow(\downarrow)}^f}{\sigma^f}\frac{I}{w}-(+)c\frac{\sigma^f}{L_f}$. For $x<-a_0$, there is

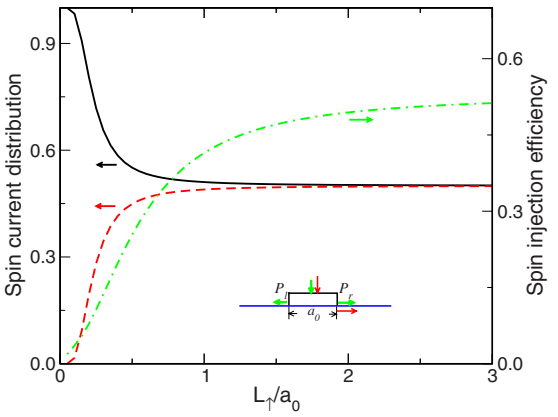

FIG. 2. (Color online) Spin-current distribution at the two edges, P_r (solid line) and P_l (dashed line), and spin-injection efficiency α (dotted-dashed line) as a function of transfer length. Red (dark gray) and green (light gray) arrows in the inset represent the total current I and the spin current $I_\uparrow - I_\downarrow$, respectively. Parameters are the same as in Fig. 1.

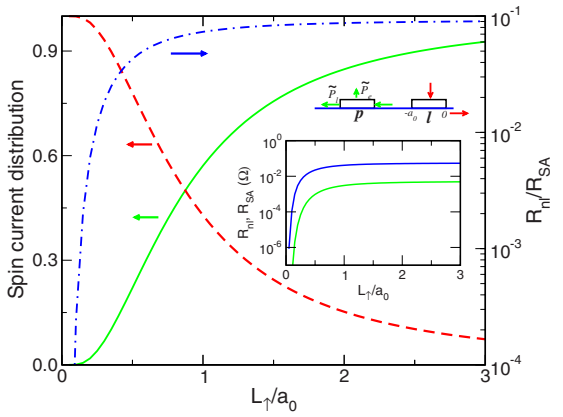

FIG. 3. (Color online) Spin-current distribution $\tilde{P}_l$ (solid line) and $\tilde{P}_e$ (dashed line) as well as ratio of the nonlocal resistance and the spin accumulation, R_{nl}/R_{SA}, at $x=-a_0$ (dotted-dashed line) as a function of the transfer length. The inset shows nonlocal resistance R_{nl} (green or light gray line) and spin accumulation R_{SA} (blue or dark gray line). Other parameters are $a_0=c_0=1$ μm.

no charge current and $\sigma_\uparrow=\sigma_\downarrow=1/2R_\square$, thus $I_s(-a_0)=\sigma_s\frac{d\mu_s}{dx}=\frac{1}{2R_\square}\frac{b}{L}$. For $x>0$, because of the dc-bias current and associated carrier injection, σ_s deviates from $1/2R_\square$,

$$\delta\sigma_s=\frac{\delta n_s}{2n_sR_\square}=\pm 1/R_\square\frac{\mu_s-\mu_0}{|\mu_0|},$$

where $\pm$ is for electrons and we have used the relation $n_s\sim|\mu_0|^2$ because of the linear dispersion in graphene. Thus

$$I_s(0)=\left(\frac{1}{2R_\square}\frac{d\mu_s}{dx}+\delta\sigma_s\frac{d\mu_0}{dx}\right)_{x=0}=\frac{1}{2}\left(I-\frac{b}{R_\square L_e}+I_0\frac{eb}{\mu_0^0}\right),$$

where $I_0=(1/R_\square)d\mu_0/dx$ is used and μ_0^0 is the Fermi level at $x=0$. The last term in the above equation becomes important (negligible) if graphene carriers are depleted (accumulated) at the contact region. At the Co/graphene contact, from their work functions, electrons will be depleted and holes will accumulate in graphene.

When $I_0=0$, i.e., the linear regime of spin injection, the spin splitting in electrochemical potential, $\mu_\uparrow(x)-\mu_\downarrow(x)$, is proportional to the ac current I, and we define the spin accumulation and the spin-injection efficiency as

$$R_{SA}(x)=\frac{\mu_\uparrow(x)-\mu_\downarrow(x)}{I},\quad \alpha=\left.\frac{I_\uparrow-I_\downarrow}{I}\right|_{z=0}. \tag{8}$$

Figure 1 shows spin-polarized currents, I_s, and spin accumulation, R_{SA}, as a function of x for different transfer lengths. We see that when the transfer lengths are much smaller than the contact size, both the spin current and accumulation concentrate at the inner edge of the circuit. When the transfer lengths are much greater than the contact size, the spin current and accumulation spread across the entire contact.

The injected spin current into the graphene will flow out at the two edges of the electrode. The relative weights of spin currents at the two edges are $P_l=(I_\uparrow-I_\downarrow)_{x=-a_0}/(I_\uparrow-I_\downarrow)_{z=0}$ and $P_r=-(I_\uparrow-I_\downarrow)_{x=0}/(I_\uparrow-I_\downarrow)_{z=0}$, where $P_l+P_r=1$. In Fig. 2, we depict P_l, P_r, and the spin-injection efficiency, α, as a function of the transfer length. We see that for $L_s/a_0<1$, most of the spin current flows to the inner edge, where the charge current is finite and the spin-injection efficiency is small. As the transfer length increases, the spin currents are equally distributed between the two edges and the spin-injection efficiency increases. Since spin-injection signals are measured in a voltage circuit next to the current circuit, it is spin accumulation and current at the outer edge, $R_{SA}(-a_0)$ and P_l, that are more important to the measurements. In literature, spin accumulation and spin current are always implicitly assumed to be symmetric at the two edges, which, as shown in Figs. 1 and 2, is valid only when $L_s/a_0\gg 1$.

IV. TRANSFER LENGTH AND SPIN DETECTION

To understand spin detection and its dependence of transfer lengths, we consider explicitly only two contacts, ***p*** with size c_0 from the voltage circuit and ***l*** with size a_0 from the current circuit, separated by d, as schematically shown in Fig. 3. The other two contacts in the voltage and current circuits can be regarded to be located at $x=-\infty$ and $x=+\infty$. The general solutions to the spin-transport equations outside the contact regions in the graphene layer are $\mu_{\uparrow(\downarrow)}=w_1+(-)b_1e^{-x/L}+(-)b_2e^{x/L}$ between ***p*** and ***l*** and $\mu_{\uparrow(\downarrow)}=w_2+(-)ce^{x/L}$ to the left of ***p***. Contact ***p***, which does not have a charge current, $I=0$, has the spin-polarized electrochemical potential $\mu^p_{\uparrow(\downarrow)}=\mu^p_0+(-)c^p\frac{\sigma^p}{\sigma^p_{\uparrow(\downarrow)}}e^{-z/L_f}$. The general solutions have ten unknown coefficients and can be fully determined by eight relations obtained from Eqs. (4) and (5) and two spin-conservation conditions for the two contacts. Because of spin injection in the current circuit, a finite difference in electrochemical potential between the two electrodes in the voltage circuit will be developed, $\mu^p_0-w_2$, where w_2 is the electrochemical potential at $x=-\infty$. The nonlocal resistance is defined as

$$R_{nl}=\frac{\mu^p_0-w_2}{I}. \tag{9}$$

It is easy to verify that $\mu^p_0-w_2$ flips the sign if electrode ***p*** reverses its magnetization. Experimentally the nonlocal re-

sistance is often defined as $R^e_{nl}=\frac{\mu^p_0(p)-\mu^p_0(ap)}{I}$, where $\mu^p_0(p)[\mu^p_0(ap)]$ represents the electrochemical potential when the magnetization of electrode $\boldsymbol{p}$ is parallel (antiparallel) with that of electrode $\boldsymbol{l}$. Hence $R^e_{nl}=2R_{nl}$.

Since electrode $\boldsymbol{p}$ is used for probing the spin accumulation at electrode $\boldsymbol{l}$, it is desired that the measured signal be independent of properties of electrode $\boldsymbol{p}$. Spin currents in electrode $\boldsymbol{p}$ come from the spin current at electrode $\boldsymbol{l}$, which flows into electrode $\boldsymbol{p}$ at its right edge and then splits into two portions: one into graphene at the left edge with a percentage of $\tilde{P}_l$ and the other into the electrode with a percentage of $\tilde{P}_e$, $\tilde{P}_l+\tilde{P}_e=1$. We plot in Fig. 3 $\tilde{P}_l$, $\tilde{P}_e$, and R_{nl}/R_{SA} as a function of the transfer length. We find that when $L_s/a_0>1$, $\tilde{P}_e$ is small, and both R_{nl} and $R_{SA}(-a_0)$ depend very weakly on L_s with their ratio remaining constant. Whereas for $L_s/a_0<1$, $\tilde{P}_e$ is large. Both the nonlocal resistance and the spin accumulation depend strongly on L_s, and the ratio between them also is strongly varying with L_s, suggesting that the measured nonlocal resistance does not accurately reflect the spin accumulation at electrode $\boldsymbol{l}$. This indicates that a "leaking" spin current into the electrode is undesirable for a reliable measurement of spin signals. This resembles measurement of electrical voltage: a good voltmeter must have a very large resistance (small leaking current).

V. NONLINEAR SPIN TRANSPORT: COMPARISON WITH EXPERIMENT

To quantitatively model experimental measurements, we consider both the electrodes in the current circuit and the electrode in the voltage circuit that is next to the current circuit, as schematically shown in Fig. 4(a). Again we write the general solutions of μ_s in different regions and determine the 15 unknowns in these solutions. The sizes of electrodes $\boldsymbol{p}$, $\boldsymbol{l}$, and $\boldsymbol{r}$ are c_0, a_0, and b_0, respectively, and the inner-edge distance is d between $\boldsymbol{l}$ and $\boldsymbol{r}$, and d' between $\boldsymbol{p}$ and $\boldsymbol{l}$. The transparent-interface device in Ref. 6, with its signals plotted in Fig. 4(a), has dimensions of $a_0=b_0=c_0=60$ nm, $d=d'=1$ μm, $w=2$ μm, and the graphene sheet resistance is $R_\square=3.3$ kΩ for p type, $R_\square=1.7$ kΩ for n type. The device with Al_2O_3 in Ref. 5, with its signals plotted in Fig. 4(b), has dimensions of $a_0=90$ nm, $b_0=140$ nm, $c_0=250$ nm, $d=1.5$ μm, $d'=0.5$ μm, and $w=0.5$ μm, and the graphene sheet resistance is $R_\square=910$ Ω. Since the thickness of the electrodes is comparable to or less than the bulk spin-diffusion length, L_f is assumed to be the thickness of the electrode, 80 nm in Fig. 4(a) and 50 nm in Fig. 4(b). We fix $L_\downarrow/L_\uparrow=1.3$ and fit the data by adjusting $L_\uparrow$. Good agreement between theory and experiment is obtained for the transparent-interface device when the transfer lengths $L_\uparrow=40$ nm is used for n-type and $L_\uparrow=33.5$ nm for p-type graphene. These lengths correspond to the contact resistance of 43 Ω and 69 Ω for n type and p type, respectively, which is in the range of measured contact resistance for the same device and consistent with the observed larger contact resistance in p type than in n type.[20] Thus the electron-hole asymmetry for structures with a transparent

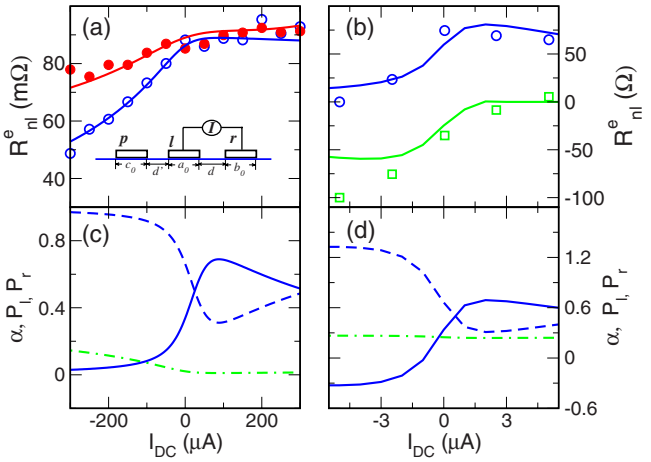

FIG. 4. (Color online) Nonlocal resistance for device structures (a) with a transparent interface and (b) with an Al_2O_3 interfacial layer as a function of dc-bias current. Solid (open) circles in (a) are experimental data for the n-type (p-type) graphene when electrode $\boldsymbol{p}$ flips its magnetization (Ref. 6). Blue or dark gray circles (green or light gray squares) in (b) are for experimental signals when electrode $\boldsymbol{l}(\boldsymbol{p})$ flips its magnetization (Ref. 5). Solid lines in (a) and (b) are theoretical results. Panels (c) and (d) are calculated spin-injection efficiency α (dotted-dashed lines), spin-current distribution P_l (solid lines), and P_r (dashed lines) at left and right edges of electrode $\boldsymbol{l}$ for p-type graphene when the electrodes magnetizations are parallel for the devices in panels (a) and (b), respectively. All three Co electrodes have $\sigma^f=1.7\times10^5$ and $(\sigma^f_\uparrow-\sigma^f_\downarrow)/\sigma^f=0.5$. The spin-diffusion length in graphene is 1 μm.

interface can be attributed to their different contact resistances for n- and p-type graphene. For the device with Al_2O_3, the transfer length used is 800 nm, which corresponds to a contact resistance of 16.3 kΩ for the 90 nm electrode, again consistent with the contact-resistance measurements of the same device.[13] We see from panels (c) and (d) that the dc-bias current greatly modifies P_l and P_r with $P_l+P_r=1$ maintained, i.e., redistributes the spin currents between the two edges. The negative P_l in Fig. 4(d) indicates the sign change in the spin current. The current dependence of P_l and R^e_{nl} have a very similar shape, suggesting that the observed current-dependent nonlocal resistance is due mainly to the electric-field-induced spin-current redistribution rather than the change in spin-injection efficiency, which depends on the current weakly, as shown in panels (c) and (d).

VI. CONCLUSIONS

In summary, we have introduced a concept of spin-dependent transfer length in graphene-based spintronic device structures and developed a unified theory to describe spin-injection signals and their dependence on a dc-bias current. The spin-dependent transfer length, which measures the length required for a current to change from lateral in 2D graphene to vertical in a 3D electrode, largely determines efficacy of spin injection and detection. The theory quantita-

tively explains seemingly conflicting experimental measurements in these devices by different groups and indicates that the observed dc-bias dependence is due mainly to redistribution of the spin current near the ferromagnetic electrode but not to a dc-bias-induced change in the spin-injection efficiency, as believed in the literature. The excellent agreement between theory and experiment underscores the necessity of the spin-dependent transfer length in describing graphene and other lateral spintronic device structures.

ACKNOWLEDGMENTS

We are grateful to M. A. Berding, W. Han, C. Jozsa, R. Kawakami, and J. Shi for useful discussions. This work was supported by the U.S. government. Z.G.Y. also acknowledges financial support from the Office of Basic Energy Sciences, Department of Energy, under Grant No. DE-FG02-06ER46325.

*zhi-gang.yu@sri.com

[1] E. W. Hill, A. K. Geim, K. Novoselov, F. Schedin, and P. Blake, IEEE Trans. Magn. **42**, 2694 (2006).
[2] N. Tombros, C. Jozsa, M. Popinciuc, H. T. Jonkman, and B. J. van Wees, Nature (London) **448**, 571 (2007).
[3] K. S. Novoselov, A. K. Geim, S. V. Morozov, D. Jiang, Y. Zhang, S. V. Dubonos, I. V. Grigorieva, and A. A. Firsov, Science **306**, 666 (2004).
[4] A. K. Geim and K. S. Novoselov, Nature Mater. **6**, 183 (2007).
[5] See, for example, A. Fert, Rev. Mod. Phys. **80**, 1517 (2008).
[6] See, for example, D. D. Awschalom and M. E. Flatté, Nat. Phys. **3**, 153 (2007).
[7] G. Schmidt, D. Ferrand, L. W. Molenkamp, A. T. Filip, and B. J. van Wees, Phys. Rev. B **62**, R4790 (2000).
[8] E. I. Rashba, Phys. Rev. B **62**, R16267 (2000).
[9] D. L. Smith and R. N. Silver, Phys. Rev. B **64**, 045323 (2001).
[10] A. Fert and H. Jaffreś, Phys. Rev. B **64**, 184420 (2001).
[11] Z. G. Yu and M. E. Flatté, Phys. Rev. B **66**, 201202(R) (2002); **66**, 235302 (2002).
[12] M. Johnson and R. H. Silsbee, Phys. Rev. B **37**, 5312 (1988).
[13] C. Jozsa, M. Popinciuc, N. Tombros, H. T. Jonkman, and B. J. van Wees, Phys. Rev. B **79**, 081402(R) (2009).
[14] W. Han, W. H. Wang, K. Pi, K. M. McCreary, W. Bao, Y. Li, F. Miao, C. N. Lau, and R. K. Kawakami, Phys. Rev. Lett. **102**, 137205 (2009).
[15] J. Hamrle, T. Kimura, Y. Otani, K. Tsukagoshi, and Y. Aoyagi, Phys. Rev. B **71**, 094402 (2005).
[16] T.-S. Kim, B. C. Lee, and H.-W. Lee, Phys. Rev. B **78**, 214427 (2008).
[17] See, e.g., H. H. Berger, Solid-State Electron. **15**, 145 (1972).
[18] C. Józsa, M. Popinciuc, N. Tombros, H. T. Jonkman, and B. J. van Wees, Phys. Rev. Lett. **100**, 236603 (2008).
[19] P. C. van Son, H. van Kempen, and P. Wyder, Phys. Rev. Lett. **58**, 2271 (1987).
[20] W. Han, K. Pi, W. Bao, K. M. McCreary, Y. Li, W. H. Wang, C. N. Lau, and R. K. Kawakami, Appl. Phys. Lett. **94**, 222109 (2009).